Stem Cell Research & Therapy

RESEARCH

Open Access

Lyophilized MSC-EVs attenuates COVID-19 pathogenesis by regulating the JAK/STAT pathway

Nesrine Ebrahim[1,2,3,4†], Hajir A. Al Saihati[5*†], Zahraa Alali[6], Sabry Younis Mohamed Mahmoud[7], Ali A. Rabaan[8,9,10], Arigue A. Dessouky[11], Rabab F. Salim[12], Ashraf A. Shamaa[13], Ahmed N. Abdallah[14], Nehal M. Elsherbiny[15], Gamal Othman[16], Abdelnaser A. Badawy[17], Gianpiero Di Leva[18] and Omnia A. Badr[19*]

Abstract

Background The JAK/STAT signaling pathway plays a crucial role in the release of interferons (IFNs) and the proinflammatory response during SARS-CoV-2 infection, contributing to the cytokine storm characteristic of severe COVID-19 cases. STAT3, a key protein in this pathway, has been implicated in promoting inflammation, making its inhibition a potential therapeutic strategy to mitigate disease severity. Mesenchymal Stem Cell-derived Extracellular Vesicles (MSC-EVs), enriched with immunomodulatory and antiviral miRNAs, offer a promising therapeutic approach by modulating gene expression and regulating inflammatory responses. This study investigates the ability of Lyophilized MSC-EVs to inhibit the JAK/STAT pathway, highlighting their potential application in COVID-19 management.

Methods Male Syrian hamsters were used as an experimental model, housed under controlled laboratory conditions. SARS-CoV-2 (hCoV-19/Egypt/NRC-03/2020) was propagated in Vero E6 cells, and viral titers were determined using plaque assays. Hamsters were intranasally challenged with the virus and treated intraperitoneally with 0.5 mL of lyophilized human Wharton's jelly-derived MSC-extracellular vesicles (MSC-EVs). Histopathological evaluations were performed on lung tissues using H&E, Masson's trichrome, and immunohistochemical staining. Morphometric analyses were conducted to assess lung injury and fibrosis. Western blotting was employed to evaluate protein expression. All procedures adhered to ethical and biosafety guidelines.

Results The administration of MSC-EVs significantly upregulated the expression levels of miRNA-146a, miRNA-124, miRNA-155, miRNA-29b, miRNA-7, miRNA-145 and miRNA-18a compared to their levels in the COVID-19 group, suggesting a targeted release of miRNA-cargo from the MSC-EVs into the lung tissue of the animals. MSC-EVs impaired the activation of the STAT3/STAT1 signaling pathway and reduced the cytokine storm and coagulopathy associated with COVID-19.

Conclusions These findings suggest that MSC-EVs have the potential to effectively mitigate the pathogenesis of COVID-19 by targeting the JAK/STAT signaling pathway. Further research is needed to fully understand

[†]Nesrine Ebrahim and Hajir A. Al Saihati have contributed equally to this work and first co-authors.

*Correspondence:
Hajir A. Al Saihati
hajirsh@uhb.edu.sa
Omnia A. Badr
omnia.badr@fagr.bu.edu.eg
Full list of author information is available at the end of the article

the mechanisms underlying the therapeutic effects of MSC-EVs and their clinical application in combating the COVID-19 pandemic.

Keywords COVID-19, MSCs-EVs, JAK/STAT signaling pathway, MicroRNA

Introduction

The COVID-19 pandemic was caused by the highly contagious SARS-CoV-2 virus, causing serious problems for the international health care systems [1]. The association between SARS-CoV-2 and the renin-angiotensin system (RAS) is a critical constituent of viral pathogenesis. The angiotensin-converting enzyme 2 (ACE2) considered a crucial part of the RAS and produced in many organs promoting the entry of virus into host cells [2, 3]. ACE2 is crucial for preserving tissue microcirculation and controlling inflammation via the RAS in addition to its function in viral entry [4]. Angiotensinogen is changed by the RAS into angiotensin I (Ang I), which is then broken down by ACE to create bioactive angiotensin II (Ang II) [5]. Additionally, Ang I is changed by ACE2 into Ang (1–9), which can then be changed into angiotensin 1–7 (Ang 1–7) [5].

Derivatives of angiotensin mediate several signaling pathways in the body. For example, Ang II is a profibrotic, proinflammatory, and vasoconstrictor mediator [3]. Therefore, COVID-19's disruption of the ACE2 pathway exacerbates these effects by making lung fibrosis, inflammation, and vascular permeability worse. The RAS critical role in COVID pathogenesis is due to the imbalance in angiotensin peptides leading to respiratory distress and other severe symptoms in patients [5]

The intracellular domains of ACE2 receptors are phosphorylated by activated Janus kinases (JAKs), which facilitates the binding of signal transducer and activator of transcription (STAT) transcription factors. STAT can enter the nucleus and detach from the receptor as a result of this phosphorylation. The cytokine storm, a hyperactive innate immune response induced by the JAK signaling cascade and driven by specific cytokines, is a critical feature of severe COVID-19 cases [6]. STAT3 has been linked to many COVID-19 consequences associated with lymphopenia as compromising antiviral immunity, increasing proinflammatory reactions and intensifying cytokine storms [7]. So, STAT3 targeting reducing the severity of COVID-19.

Mesenchymal stem cells (MSCs) can produce cytokines and immunoreceptors and exhibit immunomodulatory capabilities through MSC-derived extracellular vesicles (MSCs-EVs) to regulate the tissue microenvironment [8]. MicroRNAs (miRNAs), which are present in MSC-EVs and regulate the majority of critical physiological processes such immunological responses, apoptosis, and cell proliferation, have been shown to give MSC-EVs antiviral, antifibrotic, immunomodulatory, and tissue healing properties [9, 10]. As a result, MSC-EVs are demonstrating potential as COVID-19 therapy agents [11].

By focusing on pro-inflammatory cytokines, miR-200c-3p and miR-26b-5p, for instance, have been demonstrated to regulate inflammatory responses and lessen inflammation, which is essential for tissue healing [12]. Additionally, in inflammatory tissues, miR-125b-5p maintains the balance between cell survival and death via controlling apoptosis [13]. Additionally, it has been discovered that miR-98-5p and let-7f-5p play a significant role in reducing lung inflammation and fostering healing in COVID-19 patients, while miR-27b-3p enhances MSC regeneration, which is beneficial for individuals who have sustained significant lung damage from the virus [14].

In this work, we investigated the association between MSC-EVs and COVID-19 by modulating miRNAs, altering the STAT3/STAT1 pathway and reducing the cytokine storm associated with the disease.

Materials and methods

Experimental animals

Male adult Syrian hamsters, 100–150 g in weight, were obtained from Egypt's National Research Center (NRC). The animals were kept in tidy cages with free access to drinking water and normal rodent feed. Animals were familiarized with an environment that featured daylight cycling (12-h cycles beginning at 8:00 AM) and room temperature (23 °C). Animals were handled in accordance with international and national ethical standards (Ethical Guidelines for the Use of Animals in Research, 2019).

The work was authorized by the National Research Council (NRC) ethical committee (approval number: NRC-20074), and all methods and experiments followed the approved protocol. Under controlled laboratory and biosafety conditions, live viral infection studies were conducted in negative pressure-based level 3 isolators (PLAS LABS, Lansing, MI). Additionally, all the experimental procedures adhered to the guidelines and were approved by the institutional review board (BUFVTM 13–04–22, Faculty of Veterinary Medicine, Benha University, Egypt). The National Institutes of Health Guide for the Care and Use of Laboratory Animals (NIH publication 85–23, revised 2011) was strictly followed for all experiments.

SARS-CoV-2 viral preparation

hCoV-19/Egypt/NRC-03/2020, a strain of the SARS-CoV-2 virus, was cultivated at an MOI of 0.005 in Vero E6 cells (ATCC No. CRL-1586) maintained in a humid incubator at 37 °C with 5% CO2 and subjected to daily microscopic examination. This sample has the GISAID accession number EPI_ISL_430819. The virus-infected culture supernatant was extracted 72 h after infection and centrifuged twice for 15 min at 4 °C for clarification, after which the supernatant was aliquoted and titrated using a plaque assay [15]. VERO-E6 cells were infected in a 6-well cell culture plate using the virus, which was then serially diluted ten times in cell maintenance medium and incubated for one hour at 37 °C with 5% CO2. The uninfected wells served as controls. After infection, the plates were cultured for 72 h at 37 °C with 5% CO_2, after which 3 ml of overlayer medium with agarose were added to each well, and the plates were held at room temperature for solidification. Fixation and virus inactivation were carried out using a 10% formalin solution for 1 h. Following fixation, the overlay was removed, and a 0.1% crystal violet solution was applied for staining. Viral plaques were observed as clear, uncolored specimens against a violet background of stained cells. The following formula was used for viral titer determination: plaque-forming units (PFUs)/ml = number of plaques × virus-injected volume × viral dilution × 10.

MSCs-extracellular vesicles (MSCs-EVs)

Human Wharton's jelly-derived Mesenchymal Stem cell-derived lyophilized exosomes were purchased from Bioluga® (Canada) with Certificate ID: TU35-5ZN4. The EVs were reconstituted in 5 ml distilled water, where 1 ml contained MSC–EVs derived from 0.5 × 106 MSCs [16, 17]. Lyophilization process as stated in the COA of the product was by freeze drying and sublimation using a cryoprotectant stabilizer which improves its stability and temperature tolerance and increases the shelf life and extends preservation periods of exosomes without losing its intrinsic cargo or harmful effects on the exosomal membranes[16].

Hamster infection challenge

A viral microneutralization assay was used to confirm the seronegative status of male Syrian hamsters. Ketamine-xylazine was used to individually anesthetize Syrian hamsters (K, 100 mg/kg; X, 10 mg/kg). Hamsters were intranasally challenged with 100 µL of 50 µL of SARS-CoV-2 and observed for an additional 7 days [18]. An intraperitoneal injection of 0.5 ml of MSCs-EV was given to the corresponding group 8 h after infection.

Animal experimental design

After two weeks of acclimatization, 28 male Syrian hamsters were randomly divided into three groups according to Al Saihati [15]:

Group I (control group; n = 14): The hamsters were divided equally into two subgroups:

Subgroup Ia: Standard laboratory conditions without any intervention.

Subgroup Ib: Single intraperitoneal injection of 0.2 ml of phosphate-buffered saline.

Group II (Covid group; n = 7): Hamsters were sacrificed after 7 days of infection challenge (at the end of the experiment).

Group III (MSC-EVs group; n = 7): Eight hours after infection challenge, the hamsters were injected intraperitoneally with 0.5 ml of MSC-EVs per rat at a concentration of 100 µg protein/ml [19].

Body temperature and weight were measured daily for each group. Any changes in mortality or morbidity were noted. The nasal washes of the anesthetized animals were taken at 1, 3, 5, and 7 days after infection.

After 7 days from the viral challenge, the hamsters were starved for 12 h before anesthesia. We carried out euthanasia of the animal using a two-step procedure in full compliance with our institutional guidelines for humane animal research. First, the animal were administered an intramuscular injection of a combination of ketamine (100 mg/kg) and xylazine (10 mg/kg) to induce deep surgical anesthesia. Once the animals were confirmed to be in a deep plane of anesthesia, as evidenced by the loss of withdrawal reflexes and lack of response to stimuli, we proceeded with euthanasia. Euthanasia was performed by exsanguination (cardiac puncture) through the collection of a terminal blood sample via the retro-orbital sinus, which results in the rapid depletion of blood volume and death of the animal under deep anesthesia. The entire euthanasia process was carried out by trained personnel in a dedicated euthanasia room, using techniques that minimize any potential pain or distress to the animals. All procedures were reviewed and approved by our Institutional Animal Care and Use Committee (IACUC) to ensure they adhered to the highest standards of humane animal research and have been reported in line with the ARRIVE 2.0 guidelines. [20]. Arterial perfusion fixation was carried out through the left ventricle while the hamsters were immobilized. Three sections of lung tissues were separated. For histopathological analyses, the first component was fixed in 10% formaldehyde, cleaned, dried, and embedded in paraffin blocks. To evaluate the virus titers in each collected organ, the second half was stored in RNeasy prior to being homogenized. The third portion was set aside in SDS buffer.

Bioinformatic analysis

In the current study, we identified miRNAs enriched in MSC-EVs by leveraging EVmiRNA (http://bioinfo.life.hust.edu.cn/EVmiRNA#!/) and ExoCarta (http://www.exocarta.org/), which provide comprehensive databases of EV-associated miRNAs. Additionally, we investigated their potential interactions with JAK/STAT signaling target genes, as well as their potential target COVID-19 receptors using miRTarBase (http://mirtarbase.mbc.nctu.edu.tw/php/index.php), which provides experimentally validated miRNA-target interactions (Table 1). These analyses provide evidence supporting the presence of the miRNAs studied in MSC-EVs and their potential regulatory relationship with JAK/STAT signaling and covid-19 pathogenesis.

Quantitative real-time PCR for miRNAs

miRNAs were extracted from lung tissue using Sigma´s mirPremier microRNA Isolation Kit. Following the manufacturer's instructions, cDNA was synthesized from miRNAs using an Invitrogen NCode VILO miRNA cDNA Synthesis Kit and a Bio-Rad T100 Thermal Cycler. U6 was used as an internal control for miRNA quantification. The miRNA primer pairs used for the amplification of miRNA-146a,miRNA-124, miRNA-155, miRNA-21, miRNA-29b, miRNA-7, miRNA-145 miRNA-18a, miRNA-30c, and U6 were purchased from Genwez (New Jersey, USA) (Table 2). For RT–qPCR, Maxima SYBR Green/ROX qPCR master mix [2x] (Thermo Scientific, USA) was utilized according to the methods of Ebrahim et al. [21]. The equation RQ $= {}^{2-\Delta\Delta Ct}$ was used to calculate the relative gene expression ratios (RQs) between the treated and control groups.

Histopathological analysis

Sections of paraffin were hydrated and deparaffinized. The sections were blocked and subsequently treated with primary anti-STAT1 (monoclonal mouse antibody, Catalog No. ABIN239822), anti-STAT3, and PAI-1 (rabbit polyclonal to API-1, concentration of 5 µg/ml, ab66705, Abcam) after endogenous peroxidase activity was suppressed using 10% hydrogen peroxide. Anti-Ang1-7 (A 779, ab142820, Abcam) and anti-CD105 (rabbit polyclonal, AA 58–110; Catalog No. ABIN707561) were used. Following phosphate buffer washing, the slides were coated with biotinylated goat anti-rabbit secondary antibody IgG H&L (HRP; ab6721). Using diaminobenzidine as a chromogen for visualization, the slides were treated with labeled avidin–biotin peroxidase for the purpose of localizing the immunological reaction [22]. To evaluate fibrosis, 4–6 µm thick paraffin slices were placed on glass slides and stained with H&E and Masson's trichrome. H&E-stained fixed sections were dehydrated with increasing concentrations of ethanol. The dehydrated sections were rinsed twice in distilled water and subjected to H&E staining. Two blinded expert investigators used a Leica DMR 3000 light microscope to examine, analyze, and image the lung sections [23].

Morphometric study

Two experienced pathologists evaluated H&E, Masson's trichrome, and immune-stained sections without knowledge of the experiment. Morphometric measurements were performed on at least two hamster sections using ImageJ® Version 1.52a28 and Fiji ImageJ [24]. Three non-overlapping fields were examined from each area. To quantify lung tissue pathology, Huang, Shi et al.'s 2022 lung injury rating system was used. The alveolar wall thickness, congestion, pulmonary edema, bleeding, and neutrophil infiltration into the airspace or vessel wall

Table 1 MSC-EV miRNA IDs from the EVmiRNA database, their expression levels as RPM level, JAK/STAT signaling target genes, miRTarBase IDs, and their potential COVID-19 receptor targets

Selected miRNA	EVmiRNA ID	Expression (RPM) in MSC-EVS	Target genes related to JAK/STAT Signaling pathway	miRTarbase ID	Target covid receptors
miRNA-146a	hsa-miR-146a-5p	2,787.46	IL-8, EGFR, STAT1, TNF-α, NFKB1, TLR4, TGFB,	MIRT021220	ITGB2
miRNA-124	hsa-miR-124-3p	222.74	STAT3, IL6, IL8, NFKB1, TGFB	MIRT022979	ITGA3
miRNA-155	hsa-miR-155-5p	1,570.55	STAT3, IL6, TNF-α, IL8, STAT1, NFKB1	MIRT020864	ITGB4
miRNA-21	hsa-miR-21-5p	180,479.10	STAT3, NFKB1, TLR4, TGFB	MIRT440420	ITGB8
miRNA-29b	hsa-miR-29b-3p	24.71	STAT3, NFKB1, TGFB	MIRT438919	ITGB1
miRNA-7	hsa-miR-7-5p	2,915.84	STAT3, TNF-α, TLR4, TGFB	MIRT755409	ACE2
miRNA-145	hsa-miR-145-3p	542.8	TNF-α	MIRT735820	NRP1
miRNA-18a	hsa-miR-18a-5p	6.37	STAT3, TNF-α, TGFB	MIRT313685	ITGA2
miRNA-30c	hsa-miR-30c-5p	1,639.91	JAK1, TGFB	MIRT682086	ITGA3

Table 2 Sequences for primers

miRNA	Forward	Universal reverse	Accession
ACE2	TGCAATGGTGAATCAGGGCT	GGCAGACCACTTTCCGATCA	XM_005074209.3
IL-8	CTCCAAACCTTTCCACCCCA	TTCTCAGCCCTCTTCAAAAACT	NM_000584.4
INF-R1	TCAGCAAGTGTCGCAAGCTA	TGTGGCTGCAAGTTCTCGAT	XM_040750494
INF-R2	GAACTAGAAGCCACCGGGTC	TTTCACCCGGCCTTGGTATC	XM_040750490
IRF3	CACAGCCGATAACAGGACACT	CCTTGAGGACATGGATCCCTTA	XM_007654273
Tissue factor	GCAAGAGCACCTGTGAGGAT	GACACCATGAAGGGCCATGA	XM_040745702.1
Beta Actin	ATGACGATATCGCTGCGCTC	CACCCACGTACGAGTCCTTC	XM_013120404.3
miRNA-146a	GTTTGGTGAGAACTGAATTCCA	GTGCAGGGTCCGAGGT	MIMAT0023774
miRNA-124	GTTTAAGGCACGCGGTGAA	GTGCAGGGTCCGAGGT	MIMAT0023740
miRNA-155	GTTGGGTTAATGCTAATCGTGA	GTGCAGGGTCCGAGGT	MIMAT0023788
miRNA-21	GTTTGGTAGCTTATCAGACTGA	GTGCAGGGTCCGAGGT	MIMAT0004417
miRNA-29b	GGGCTGGTTTCATATGGTG	GTGCAGGGTCCGAGGT	MIMAT0023885
miRNA-7	GTTGGTGGAAGACTAGTGATTT	GTGCAGGGTCCGAGGT	MIMAT0020368
miRNA-145	GTGTCCAGTTTTCCCAGGA	GTGCAGGGTCCGAGGT	MIMAT0000437
miRNA-18a	GGTAAGGTGCATCTAGTGC	GTGCAGGGTCCGAGGT	MIMAT0023817
miRNA-30c	GTTCTGGGAGAGGGTTGTT	GTGCAGGGTCCGAGGT	MIMAT0041161
U6	CTCGCTTCGGCAGCACA	AACGCTTCACGAATTTGCGT	Ebrahim et al., [21]

were assessed. Lung hemorrhage, lung interstitial edema, alveolar wall thickness, and inflammatory cell infiltration were graded as follows. Masson's trichrome-stained sections at ×100 were used to assess the mean area percentage [24] of the collagen fibers. The immune reactivity area percentage was also measured. The image type was changed to RGB stack-created grayscale images of each channel to distinguish immune staining. The threshold for adjusting the image was set to 0–87 for the green channel. The analysis measures the measured area, area fraction, threshold limit, and display label. IHC quantitative evaluation used the Allred score (0–1 = negative, 2–3 = mild, 4–6 = moderate, and 7–8 = extremely positive). QuPath (0.1.2) adds the percentage of positive cells and staining intensity classes (0–3) to calculate the score [25].

Western blot

Frozen lung tissues were chopped and homogenized in ice-cold RIPA lysis buffer with a protease inhibitor cocktail (4%, Roche Diagnostics, Manheim, Germany) using hypodermic needles (20G, 22G, and 26G). Lysates of lung tissue were incubated on ice for 30 min with gentle agitation. To obtain the supernatant, the lysates were centrifuged at 12,000 rpm for 30 min. The protein concentration in each sample was determined using the Folin-Lowry spectrophotometric method (Beckman Coulter Inc., Indianapolis, Indiana). Protein extracts were incubated in Laemmli buffer for 5 min at 95 °C. Next, 50 g protein samples were placed onto a 10% sodium dodecyl sulfate (SDS) polyacrylamide gel for gel electrophoresis. After that, the proteins were blotted onto polyvinylidene difluoride (PVDF) membranes (Amersham Biosciences, Bucks, United Kingdom).

To inhibit nonspecific reactions, the membranes were incubated for 1 h in 5% nonfat dry milk in 1% TBS with Tween 20. The membranes were then treated with the selected primary antibodies overnight at 4 °C (Table 3). Next, the membranes were washed three times and incubated for one hour at room temperature with the appropriate alkaline phosphatase-labeled secondary antibody (Biospes, 1:5000). ImageJ analysis software was used to perform densitometric analysis of the immunoreactive bands, while actin serving as the internal control.

Statistical analysis

Coding, tabulating, and statistical analysis were performed in GraphPad Prism 8, version 8. The data are reported as the mean ± SEM. Statistical analysis was performed using one-way ANOVA. Next, post hoc analysis was used to identify pairwise differences. A P-value < 0.05 was considered to indicate statistical significance.

Results

Therapeutic effects of MSC-EVs combat COVID-19 pathogenicity

To assess the therapeutic potential of MSC-EVs in reducing the pathogenicity of Covid-19, Syrian hamsters were intranasally infected with SARS-CoV-2

Table 3 Primary antibodies for western immunoblotting

Antibodies	Source	Type	Identifier	Dilution ratio
Anti-TGFβ1	Santa Cruz Biotechnology	Monoclonal	sc-130348	1:1000
Anti-TLR4	Santa Cruz Biotechnology	Monoclonal	sc-293072	1:1000
Anti- NFkB	Abbexa	Polyclonal	abx012874	1:1000
Anti-TNFα	Santa Cruz Biotechnology	Monoclonal	sc-52746	1:1000
Anti- JAK1	Santa Cruz Biotechnology	Monoclonal	sc-136225	1:1000
Anti-JAK2	Santa Cruz Biotechnology	Monoclonal	sc-390539	1:1000
Anti-Stat3	Santa Cruz Biotechnology	Monoclonal	sc-293151	1:1000
Anti-p-Stat3	Santa Cruz Biotechnology	Monoclonal	sc-81523	1:1000
Anti-IL-6	Santa Cruz Biotechnology	Monoclonal	sc-57315	1:1000
Anti-β-actin	Elabscience	Monoclonal	E-AB-20031	1:5000

preparations and then treated with a single intraperitoneal injection of MSC-EVs solution. First, we confirmed viral entry and replication of SARS-CoV-2 by measuring the levels of ACE2 mRNA in the lung tissues of the infected animals. Increased levels of ACE2 mRNA were specifically identified in lung tissues of the infected animals compared to controls (Fig. 1A). We also assessed the localization of MSC-EVs in lung tissues through IHC detection by measuring the levels of CD105 and CD63, a specific marker of MSC-EVs (Fig. 1B). Although fluorescent labeling is ideal for tracking MSC-EVs, a limitation of this study is the inability to use it due to regulatory constraints on the clinical-grade Bioluga® product. Instead, we relied on

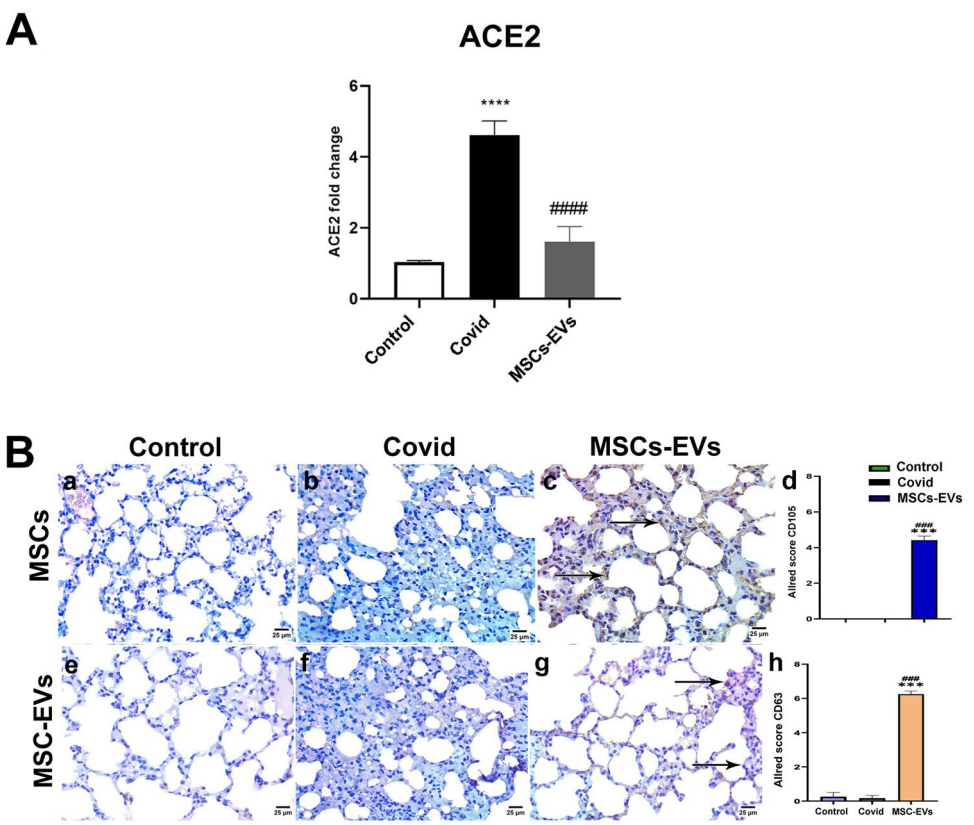

Fig. 1 **A** gene expression profiles of ACE2 lung tissues of Covid 19 hamster's model.; **B** Immunohistochemistry positive brown cytoplasmic reaction for CD63 and CD105 for localization of MSCs-EVs indicating EVs localization in lung tissues

dose-dependent marker expression, pathophysiological comparisons, and prior validations to demonstrate MSC-EV localization. The positive immune-expression of CD105 and CD63 in the MSC-EVs-treated group indicated that the EVs were exclusively localized in the lung tissues of animal infected with SARS-CoV-2 and subsequently treated with MSC-EVs.

We then determined the effect of MSC-EVs treatment on the induction of cytokines IL-8 and IL-6 which contribute to severe inflammation and tissue damage during COVID-19 [26]. The mRNA expression of both IL-8 and the protein level of IL-6 were significantly elevated in the lung tissues of SARS-CoV-2 -infected hamsters indicating an inflammatory response characteristic of COVID-19 patients (Fig. 2A). Concomitantly, a significant increase in IL-6 protein levels was also observed in the lung tissues of infected hamsters (Fig. 2B). These elevated IL-6 protein levels support the presence of an exaggerated immune response in SARS-CoV-2 infected hamsters. Remarkably, treatment with MSC-EVs resulted in a significant reduction in ACE2 and IL-8 mRNAs and IL-6 protein levels in the lung tissues of infected hamsters. Additionally, while the immune-expression of Ang 1–7, which plays a key role in regulating blood pressure and inflammation during COVID-19, was lower in the SARS-CoV-2 infected group compared to the control group, its expression was significantly higher in the MSC-EVs-treated group than in the COVID-19 group

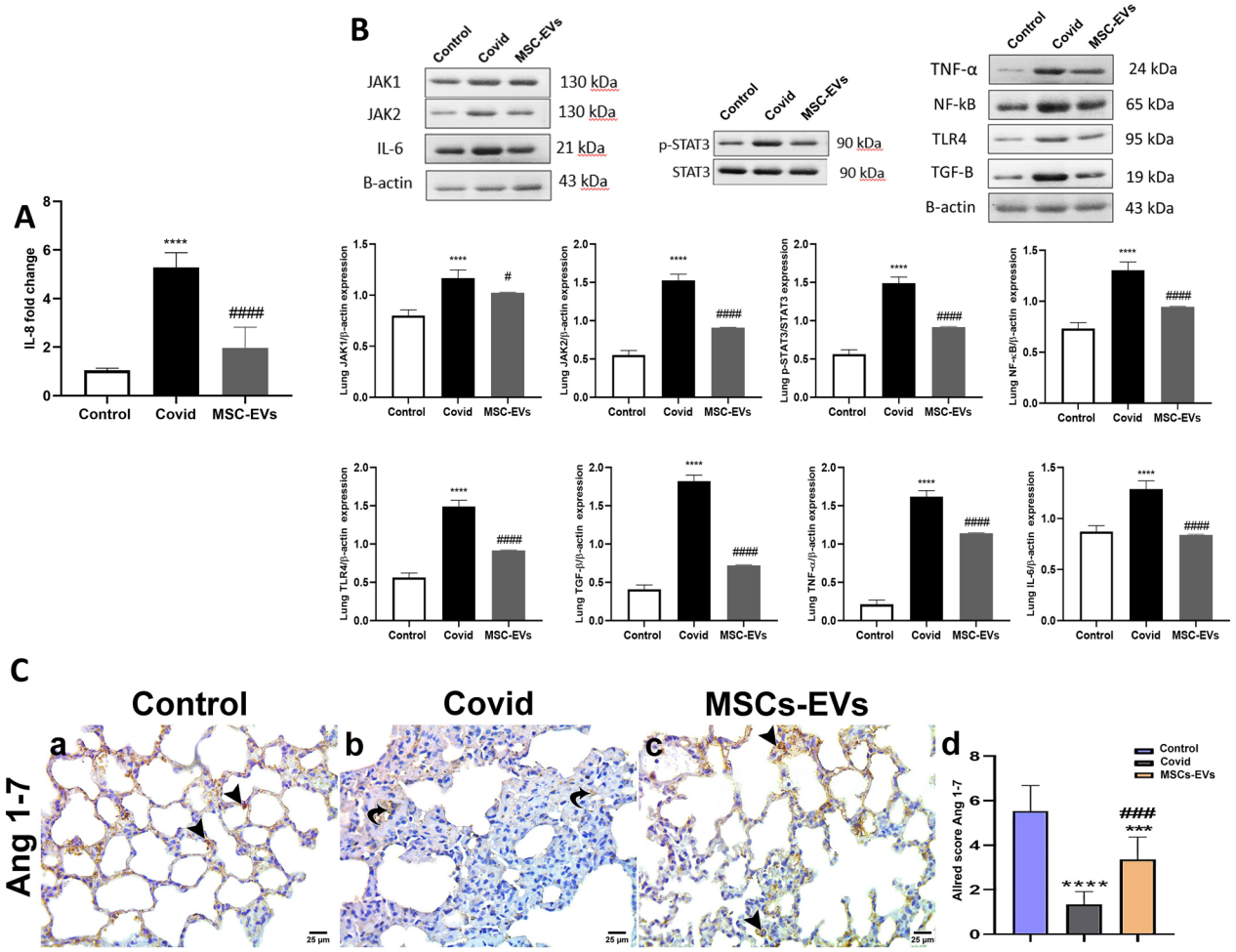

Fig. 2 **A** gene expression profiles of IL-8. **B** Effect of MSCs-EVs administration on protein levels of IL6, JAK1, JAK2, phosphorylated STAT3, TLR4, NF-κB, TGF-β and TNF-α in lung tissues from different experimental groups as detected by western blot. Data were expressed as mean ± SE. ****significant compared to Control at $p < 0.0001$, and # significant compared to COVID- 19 group at $p < 0.05$, #### at $p < 0.0001$. **c** Representative photomicrographs from Ang 1–7 immune stained lung sections showing a) Control group: negative immune reaction. b) Covid group: with intense immune reaction in consolidated lung tissue (curved arrow). c) MSCs-EVs group: negative immune reaction. d) Graph showing Allred score for Ang1-7 expression. Data are expressed as mean ± SEM.***$p < 0.001$ versus control, $p < 0.001$ versus COVID group. Allred index (0–1 = negative, 2–3 = mild, 4–6 = moderate, and 7–8 = strongly positive)

(Fig. 2C). Overall, these findings highlight the therapeutic potential of MSC-EVs in attenuating the inflammatory response associated with COVID-19 in hamsters.

MSC-EVs modulated JAK-STAT, interferon (INF), TLR4/NF-κB and inflammatory cytokines in COVID-19

Dysregulation of the JAK-STAT pathway during COVID-19 infection contributes to significantly elevated levels of various cytokines [27]. To investigate how this pathway is modulated in our model, we performed western blot analysis to assess the protein levels and activation status of its key signaling mediators. Following SARS-CoV-2 infection, we observed increased levels of JAK1 and JAK2, which were accompanied by activation of downstream transcriptional mediators, such as STAT3 and NF-κB, in the lung tissues of infected animals (Fig. 2B). Additionally, we detected elevated levels of several downstream inflammatory targets, including TLR4, TNF-α, TGF-β (Fig. 2B). To complement these findings, we also conducted immunohistochemistry for STAT1 and STAT3 in the lung tissues of infected animals (Fig. 3I). We observed elevated STAT3 protein levels following SARS-CoV-2 infection and a reduction in STAT1 immunoreactivity compared to the control group. Notably, the administration of MSC-derived extracellular vesicles (MSC-EVs) normalized or reduced the levels and activation of all JAK-STAT pathway components that were analyzed. Furthermore, we assessed the impact of SARS-CoV-2 infection on the interferon (INF) signaling pathways. We observed a significant increase in the mRNA levels of INF-R1 and IRF3 in lung tissues of infected animals compared to controls (Fig. 3II), while no significant changes were noted for INF-R2. Treatment with MSC-EVs led to a marked reduction in the expression of INF-R1 and IRF3 when compared to the COVID-19 group.

MSC-EVs increased miRNA levels in the infected lungs

miRNA in EVs plays a pivotal role in cell-to-cell communication and can modulate the inflammatory response of recipient cells by regulating gene expression at the post-transcriptional level [28]. To investigate the contribution of EV-miRNA cargo in modulating the JAK/STAT signaling pathway in our COVID-19 model, we performed RT-qPCR to assess the expression of several miRNAs that have been previously implicated in COVID-19 pathogenesis. (Fig. 4). With the exception of miR-21 and miR-30c, RT–qPCR revealed that the expression levels of miRNA-146a, miRNA-124, miRNA-155, miRNA-29b, miRNA-7, miRNA-145 and miRNA-18a were significantly reduced in the lung tissues after SARS-CoV-2 infection compared to control group ($p < 0.001$). Interestingly, the administration of MSC-EVs significantly upregulated the expression of all assessed miRNAs compared to their levels in the COVID-19 group ($p < 0.01$), suggesting a targeted release of miRNA-cargo from the MSC-EVs into the lung tissue of the animals.

MSC-EVs ameliorate histopathological alterations in COVID-19 hamsters

Histopathological examinations of lung tissues were conducted to evaluate changes in tissue architecture following SARS-CoV-2 infection and treatment with MSC-EVs. In the control group, H&E-stained lung sections revealed a normal lung histoarchitecture consisting of numerous patent alveoli and thin intervening interalveolar septa (Fig. 5A). These septa were predominantly covered by flat type I pneumocytes and a few type II pneumocytes, which appeared cuboidal in shape. Alveolar capillaries were also observed (Fig. 5Aa). In contrast, SARS-CoV-2-infected lungs exhibited prominent histopathological alterations with extensive areas of consolidation where obliteration of the alveolar lumens and marked thickening of the interalveolar septa were observed. Additionally, inflammatory cellular infiltration and intra-alveolar hemorrhage were also found (Fig. 5Ab). On the other hand, in the SARS-CoV-2-infected + MSC-EVs group, a marked improvement in lung tissue was observed. The majority of the alveoli displayed patent lumens and thin interalveolar septa. Some areas displayed little inflammatory cellular infiltration and residual areas of consolidation (Fig. 5A(c)).

In Masson's trichrome-stained lung sections, fine collagen fibers were observed in the interalveolar septa of the control group (Fig. 5B(a)). In contrast, SARS_CoV2 infected group exhibited abundant, intensely stained collagen fibers surrounding the bronchioles and within the extensively consolidated lung tissue (Fig. 5B(b)). After MSC-EV treatment, fine, intensely stained collagen fibers were observed in the thin interalveolar septa (Fig. 5B(c)). The mean percentage of collagen fiber deposition area for the three groups is shown in (Fig. 5B(d)). Covid-19 animals (Group II) had a significantly higher percentage of collagen fiber deposition compared to the control group. In contrast, the collagen deposition area in MSC-EVs treated animals (Group III) was significantly lower than that in Group II and closely resembled to that of the control group.

MSC-EV-modulated coagulation dysfunction associated with COVID-19 in hamsters

Tissue factor (TF) initiates the coagulation cascade, leading to blood clots formation. Notably, COVID-19 patients are prone to thrombotic events due to dysregulated coagulation[29]. Significant increase in the levels of TF was observed in the COVID-19 animal group compared to

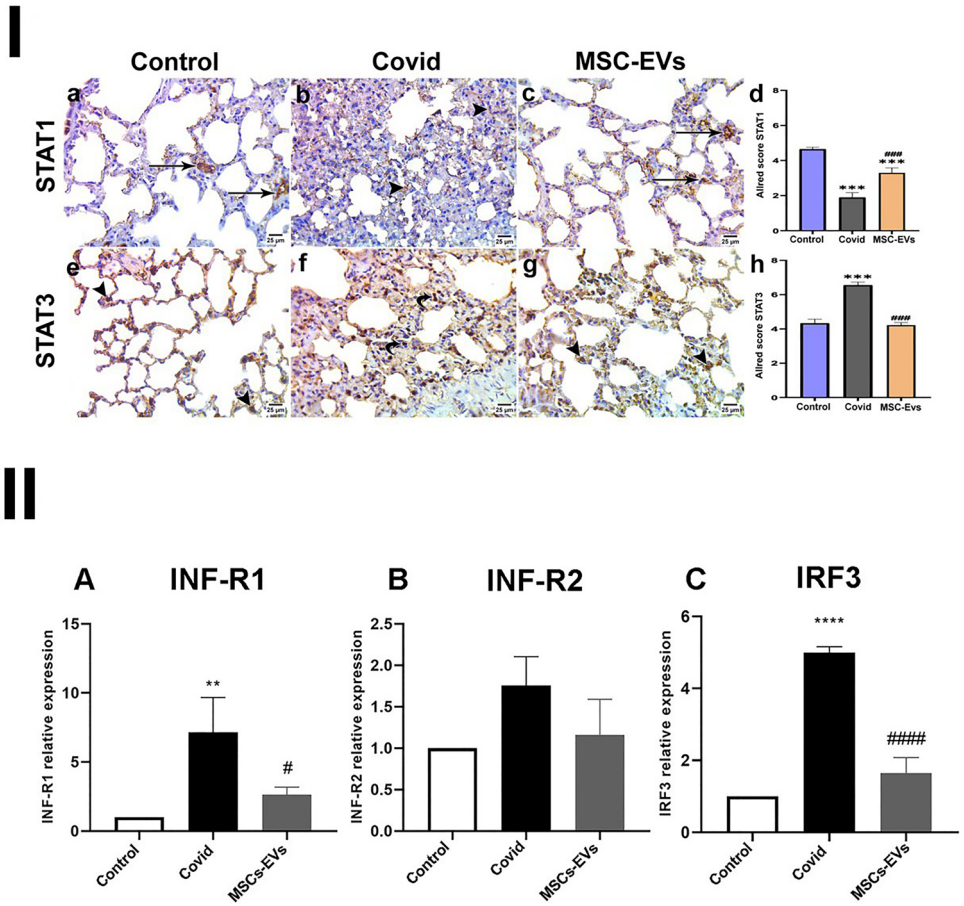

Fig. 3 **I** Representative photomicrographs from STAT1 &STAT3 immune stained lung sections showing **a** Control group: with a moderate immune reaction (arrow). **b** Covid group: with weak immune reaction in consolidated lung tissue (arrowhead). **c** MSCs-EVs group: with a moderate immune reaction (arrow). **d** Graph showing Allred score for STAT1 expression. **e** Control group: with a moderate immune reaction (arrow). **f** Covid group: with strong immune reaction in consolidated lung tissue (arrowhead). **g** MSCs-EVs group: with a moderate immune reaction (arrow). **h** Graph showing Allred score for STAT3 expression Data are expressed as mean ± SEM.***$p < 0.001$ versus control, ###$p < 0.001$ versus Covid group. Allred index (0–1 = negative, 2–3 = mild, 4–6 = moderate, and 7–8 = strongly positive). **II** Effect of MSCs-EVs administration on gene expression profiles of **A** INFR1, **B**: INFR2 and **C** IRF-3. Data were expressed as mean ± SE. ** significant compared to Control at $p < 0.01$, ****significant at $p < 0.0001$, and # significant compared to COVID- 19 group at $p < 0.05$, #### at $p < 0.0001$

the control group while treatment with MSC-EVs significantly reduced the TF levels. (Fig. 6A).

Additionally, plasminogen activator inhibitor 1 (PAI-1) regulates fibrinolysis, the process that breaks down blood clots; elevated PAI-1 levels inhibit fibrinolysis promoting prothrombotic conditions [30]. We found that COVID-19 animals exhibited higher PAI-1 immuno-expression compared to controls.

In contrast, the MSCs-EV treated group showed significantly lower PAI-1 immuno-expression than the COVID-19 group. These findings suggest that MSC-EVs can attenuate the dysregulation of both TF and PAI-1, indicating a potential antithrombotic effect that may help prevent severe thrombotic events in COVID-19 patients (Fig. 6B).

Discussion

Research on EVs derived from MSCs has shown that they have the same anti-inflammatory, immune-modulatory, and regenerative potential as their parent cells [31]. In the present study, we demonstrated that MSCs-EVs modulated miRNAs in the lung tissues of treated group, suggesting a targeted release of miRNA-cargo from the MSC-EVs into the lung tissue of the animals. Furthermore, MSC-EVs reduced the cytokine storm and coagulopathy linked to COVID-19 and inhibited the STAT3/STAT1 signaling pathway.

An imbalance in the local paracrine action of angiotensin (Ang) molecules is linked to COVID-19 invasion and replication, which results in elevated activity of Ang II and lower levels of Ang 1–7. These factors

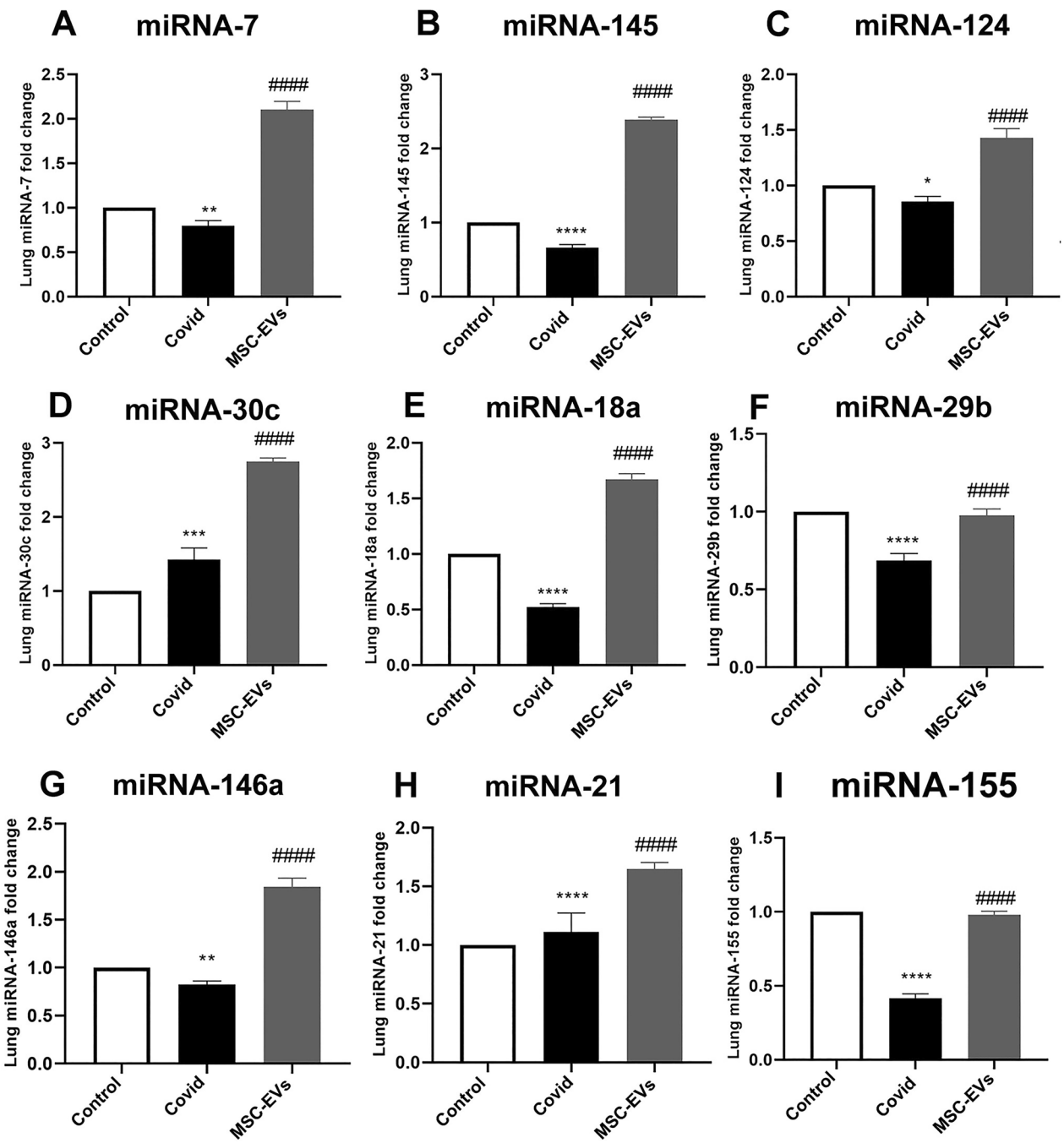

Fig. 4 Effect of MSC-EVs treatments on miRNAs expression in lung tissues of Covid-19 hamsters **A** miRNA-sevenfold change **B** miRNA-145-fold change **C** miRNA-124-fold change and **D** miRNA-30c fold change and **E** miRNA-18a fold change **F** miRNA-29b **G** miRNA-146a fold change **H** miRNA-21-fold change **I** miRNA-155 of different experimental groups. Data are expressed as mean ± SE. *significant compared to Control at $p < 0.05$, ** at $p < 0.01$, *** at $p < 0.001$, **** at $p < 0.0001$ and #### significant compared to COVID- 19 group at $p < 0.0001$

support tissue damage, fibrosis, hypercoagulability, severe inflammation, and impaired microcirculation [3]. In part by inducing IL-8, Ang II facilitates vascular permeability and neutrophil infiltration into the alveoli [3].

In accordance with these findings, the COVID-19-infected group in the present study showed increased levels of ACE2, IL6 and IL8 compared to those in the control group, causing intense inflammation, tissue damage, and fibrosis with an increased tendency for

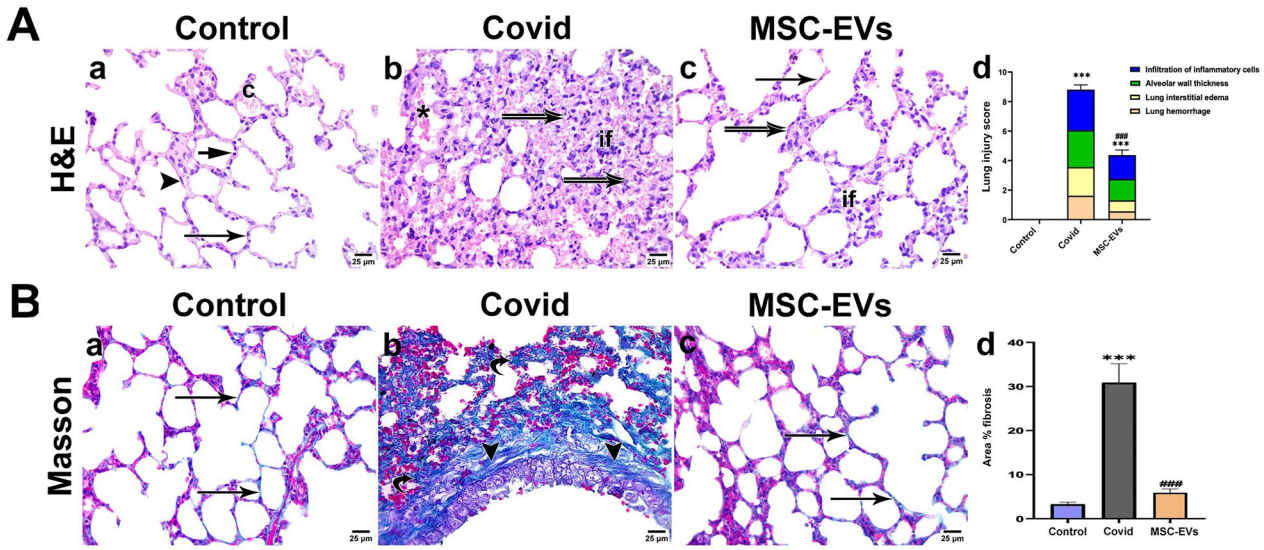

Fig. 5 **A** Representative photomicrographs from H&E-stained lung sections showing **a** Control group: patent alveoli and thin interalveolar septa (arrow) lined by flat type I pneumocytes (arrow head) and cuboidal type II pneumocytes (short arrow). An alveolar capillary (**c**) is also seen. **b** Covid group: Extensive consolidation (double arrow) with obliterated alveolar lumens, thickened interalveolar septa, inflammatory cellular infiltration (if), and intra alveolar hemorrhage (asterisk). **c** MSCs-EVs group: with patent alveolar lumens and thin interalveolar septa (arrow) and residual area of consolidation (double arrow) and inflammatory cellular infiltration (if). **d** Graph showing the lung injury scoring system. Data are expressed as mean ± SEM.***$p < 0.001$ versus control, ###$p < 0.001$ versus covid group. **B** Representative photomicrographs from Masson trichrome stained lung sections showing a) Control group: with fine collagen fibers in the interalveolar septa (arrow). **b** Covid group: with abundant, intensely staining collagen fibers surrounding the bronchioles (arrowhead) and in the extensively consolidated lung tissue (curved arrow). **c** MSCs-EVs group: with fine, intensely stained collagen fibers in the thin interalveolar septa (arrow). **d** Graph showing collagen fiber mean area percentage in the experimental groups (Masson's trichrome-stained sections). Data are expressed as mean ± SEM.***$p < 0.001$ versus control, ###$p < 0.001$ versus covid group

thrombosis. This was confirmed histologically in the form of severe alveolar hemorrhage, inflammatory cell infiltration and a thickened alveolar wall. In addition, decreased immunoreactivity of Ang1-7 and increased immunoreactivity of PAI-1 were also observed in the COVID-19-infected group. However, in the MSC-EV-treated groups, there was a significant decrease in ACE2, IL8 and IL6 compared to those in the COVID-19-infected group, and there was a significant improvement in histopathological findings in lung tissue in the form of decreased inflammatory infiltration and fibrosis with thinning of the alveolar wall. In addition, increased immunoreactivity of Ang1-7 and decreased immunoreactivity of PAI-1 were also observed.

The COVID-19 virus hinders the phosphorylation of STAT1, and its structural proteins suppress the interferon (IFN) response by antagonizing the antiviral effects of IFNs and disrupting the JAK-STAT signaling pathways they stimulate [32, 33]. This impairment of STAT1 function by COVID-19 proteins may lead to an adaptive shift toward pathways independent of STAT1, resulting in a dominant transcriptional profile reliant on STAT3 [34–36]. Dysregulation of the STAT signaling pathway induced by COVID-19 proteins is thought to underline the severe pathophysiology of COVID-19.

The COVID-19 virus triggers signaling pathways that detect viral attacks and stimulate the production of IFNs through pattern recognition receptors (PRRs). The stimulation of downstream transcription factors, such as NF-κB and IRFs, results in the synthesis of IFNs I and II and IRF3. A defense mechanism is generated when the released IFNs attach to receptors on adjacent cells. Interferon-stimulated gene products are upregulated by IFN-I and IFN-III receptors, which activate the JAK and STAT proteins. Instead, COVID-19 infection decreases IFN activity hindering the response of INF.

Consequently, protective IFN signals are not received by neighboring cells, allowing the virus to spread unhindered [37]. This finding explains the results of the present study, which demonstrated that the STAT signaling pathway was aberrantly activated in the COVID-19-infected group. In comparison to the control group, the expression of IFN-R1 and IRF3 was significantly increased with a non-significant increase in INF-R2, but the response was probably impaired, as were the levels of IL-6 and TNF-α. This occurred along with increased protein levels of STAT3, JAK1,

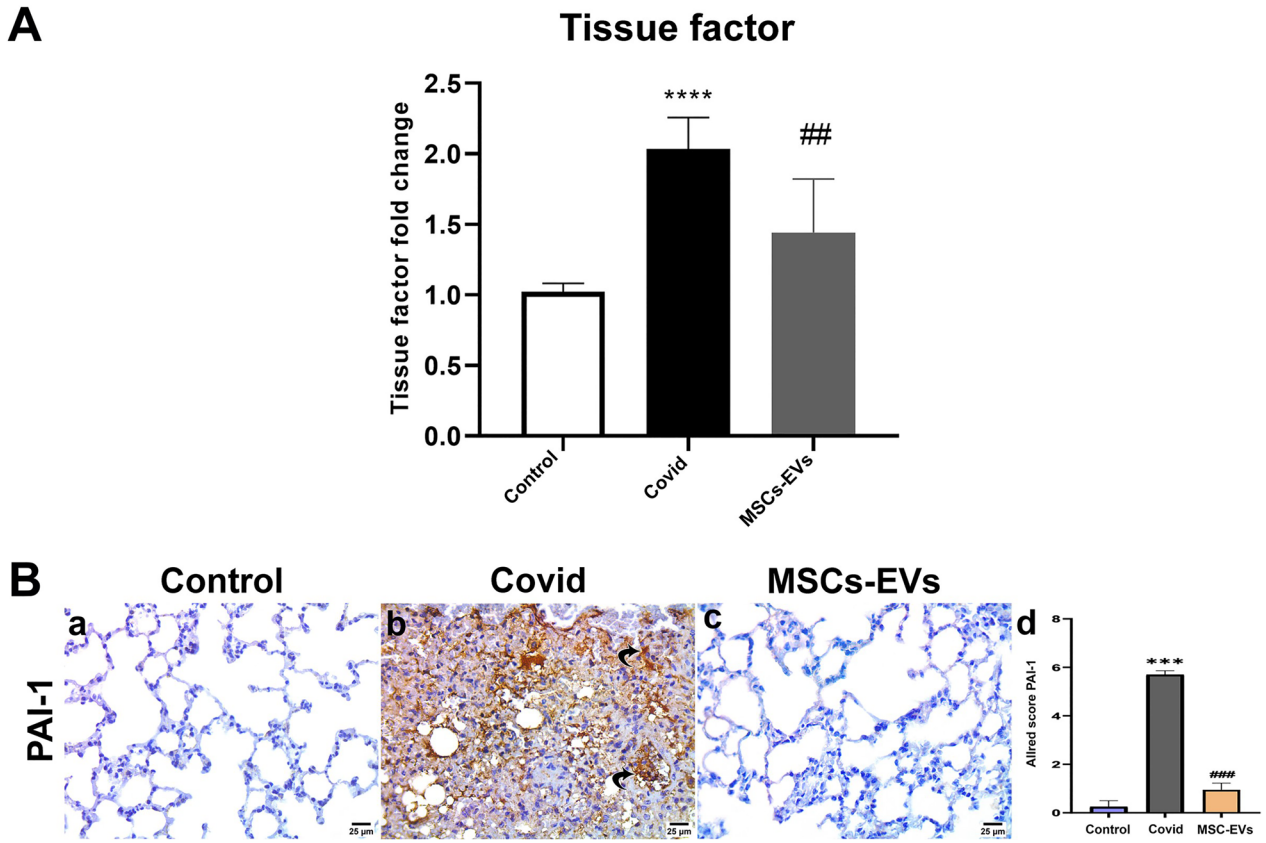

Fig. 6 **A** Effect of MSC-EVs treatments on gene expression of tissue factor (TF) in lung tissues from different experimental groups. Data are expressed as mean ± SE. ****significant compared to Control at $p < 0.0001$ and ## significant compared to COVID- 19 group at $p < 0.01$. **B** Representative photomicrographs from PAI-1 immune stained lung sections showing **a** Control group: negative immune reaction. **b** Covid group: with intense immune reaction in consolidated lung tissue (curved arrow). **c** MSCs-EVs group: negative immune reaction. **d** Graph showing Allred score for PAI-1 expression. Data are expressed as mean ± SEM.***$p < 0.001$ versus control, ###$p < 0.001$ versus COVID group. Allred index (0–1 = negative, 2–3 = mild, 4–6 = moderate, and 7–8 = strongly positive)

and JAK2 and decreased protein levels of STAT1 in the COVID-19 group. In contrast, compared with those in the COVID-19 group, the MSC-EV-treated group exhibited significantly decreased expression of IFN-R1 and IRF3 and non-significant reduction in INF-R2, but probably exhibited a proper response, as indicated by decreased levels of TNF-α. This occurred along with decreased protein levels of STAT3, JAK1, and JAK2 and increased protein levels of STAT1. Immunohistochemistry further supported these findings.

The activation of STAT3 can be occurred by both SARS-CoV-2 and Angiotensin 1–7 (Ang1-7). In SARS-CoV-2 infection, STAT3 is activated by proinflammatory cytokines such as IL-6 and TNF-α, leading to a proinflammatory cascade that contributes to immune cell recruitment, cytokine storms, and lung damage [38, 39]. Conversely, Ang1-7 activates STAT3 through the Mas receptor, triggering anti-inflammatory signaling and promoting mediators like IL-10, which counteract the harmful effects of Angiotensin II and reduce inflammation and tissue damage [40, 41]. The contrasting effects of STAT3 activation depend on the signaling context, with SARS-CoV-2 promoting inflammation and Ang1-7 mediating protection. MSC-EVs can modulate this balance by enhancing Ang1-7 levels and Mas receptor activity, shifting STAT3 activation toward its anti-inflammatory role [42]. MSC-EVs also suppress excessive STAT3 activation by inflammatory cytokines and restore the balance between STAT3 and STAT1, favoring antiviral and anti-inflammatory effects. This dual modulation of STAT3 by MSC-EVs can regulate the JAK-STAT pathway, suppress cytokine production, and regulate INF signaling in SARS-CoV-2-infected hamsters, highlighting the therapeutic potential of MSC-EVs in reducing the inflammatory response and alleviating the harmful effects associated with COVID-19 infection.

In response to proinflammatory cytokines [43], different lung cells express TF. By changing prothrombin into thrombin, which changes fibrinogen into fibrin, it aids in the production of blood clots. TF can be induced by aberrantly active STAT3. The number of infected cells may be connected to the severity of COVID-19 symptoms, as shown by disease severity [44]. Hepatocytes, adipocytes, vascular endothelial cells, and epithelial cells are among the cell types that release PAI-1 (SERPIN E1), another crucial element in diseases of blood clotting and thrombus formation. [45, 46]. According to studies, thrombosis and coagulopathy are increased in COVID-19 patients when PAI-1 and STAT3 interact [47–50].

IL-6, a central cytokine in the COVID-19-associated cytokine storm, activates STAT3, which directly enhances PAI-1 expression [51]. Similarly, TGF-β, a key driver of fibrosis, induces PAI-1 transcription, compounding the prothrombotic environment [52]. ACE2 dysfunction, resulting from SARS-CoV-2 binding, exacerbates these pathways by disrupting the renin-angiotensin system, leading to heightened inflammation and endothelial injury [53]. Furthermore, miR-30c, a microRNA known to inhibit PAI-1, has been shown to play a regulatory role in fibrinolysis but is downregulated during severe infection, further amplifying PAI-1 expression [54].

These interconnected pathways collectively promote coagulopathy, increasing the risk of thrombotic complications in COVID-19 patients. An increase in TF expression and the excretion of TF and PAI-1 into the alveolar plot cause fibrin accumulation in the bronchoalveolar system [55]. In line with these discoveries, the present study demonstrated elevated immunological expression of TGF-β and PAI-1 in the COVID-19-infected group compared with the control group. However, compared with those in the infected groups, the PAI-1 and TGF-β immune expression of the MSC-EVs-treated groups was reduced. Furthermore, lung IL-6, TLR4, TNF-α and NF-κB levels were significantly increased in the COVID-19-infected group rather than that in the control group. However, these parameters were significantly lowered in the MSC-EV-treated group than in the COVID-19 group.

Increased macrophage activation causes excessive inflammatory cytokine production in COVID-19-infected lung tissue [56–58]. According to Gupta et al., by binding to TLR4, PAI-1 triggers macrophages and initiations their production of proinflammatory cytokines [59]. Chemokines and IL-6 were produced when PAI-1 binds to TLR4 and activates NF-κB. In a feedback loop where PAI-1 contributes to positive regulation [60], IL-6 stimulates STAT3 to yield TGF-β [61], which strengthens the TLR4-mediated inflammatory response. MSC-EVs having anti-inflammatory and regulatory miRNAs, like miR-30c, which cause direct inhibition to the expression of PAI-1 [62]. Furthermore, MSC-EVs reduce the STAT3 activation and downstream PAI-1 induction via reducing the IL-6 levels [63, 64]. Moreover, the EVs may regulate the TGF-β signaling, dropping its prothrombotic and fibrotic effects [65]. Additionally, MSC-EVs may help to rebalance the renin-angiotensin system and reduce the endothelial inflammation via restoring the function of ACE2 [66]. Consequently, it seems that PAI-1 plays a vital role in the overproduction of the signaling molecules and inflammatory mediators via macrophages within the lung tissues of critically ill COVID-19 patients.

TGF-β is vital in COVID-19 as many viral diseases causing alteration of the TGF-β signaling to avoid cell death and encourage the transformation of fibroblasts into myofibroblasts. Consequently, the pulmonary fibrosis that has been developed in COVID-19 patients may be due to increased expression of TGF-β [67]. The abnormal activation of STAT3 may be involved in TGF-β activation and the resulting fibrosis in type 2 alveolar cells. Activated TGF-β also stimulates the expression of profibrotic genes that code for collagens, proteoglycans, integrins, connective tissue growth factor, and matrix metalloproteinases (MMPs) creating an environment that is favorable for fibrosis [68].

Developing as key modulators of the JAK-STAT signaling cascade, EVs-miRNAs having an exciting approach to intervention. For example, EVs- miRNA-146a increasing type I interferons (IFN-Is) synthesis activating the STAT1 and strengthens the host's antiviral defenses [69]. Additionally, the EVs'miRNA-124 and miRNA-155 efficiently suppress STAT3 production leading to reduction of the excessive inflammatory response critically ill COVID-19 patients [70, 71]. By precisely targeting IL-6, EV-miRNA-21 diminishes the hyperinflammatory response accompanying to serious viral infections, such as COVID-19 [72].

EV-miRNA-146a downregulates the immune cell chemotaxis and decreases the inflammation via IL-8 expression [73, 74]. Furthermore, EV-miRNA-29b targets JAK2, a critical checkpoint to evade an excessively active immune response, and overwhelms the JAK/STAT pathway [75]. EVs-miRNA-7 and miRNA-145 reduce the cell proliferation and inflammatory signaling by diminishing signaling via the epidermal growth factor receptor (EGFR) [76, 77]. With the intention of blockage, the STAT3 activation and limitation of the inflammatory responses, EV-miRNA-18a upsurges the production of protein inhibitor of activated STAT3 (PIAS3) [78].

EV-miRNA-30c is essential for blocking plasminogen activator inhibitor-1 (PAI-1) leading to fibrinolysins maintained and regulation of the inflammation [62]. Furthermore, EV-miRNA-146a delivers a detailed method to regulate the host response to SARS-CoV-2 infection

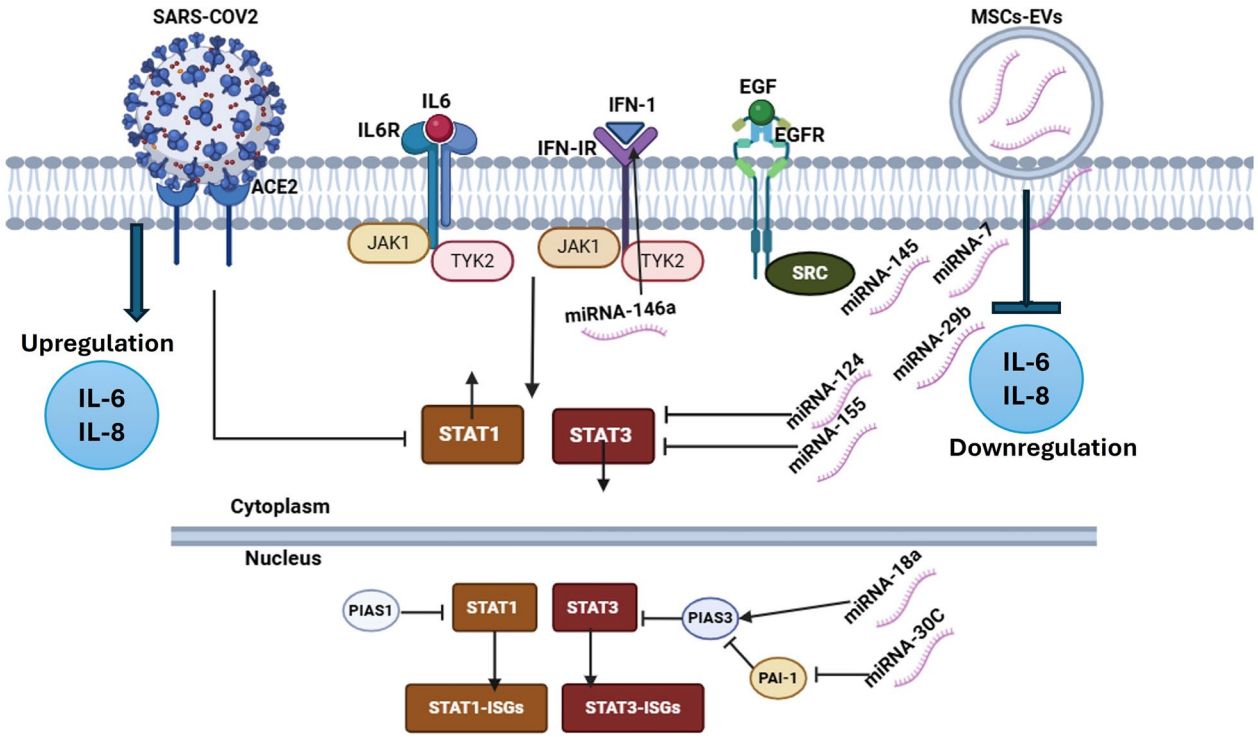

Fig. 7 The JAK/STAT signaling cascade is shown schematically in relation to SARS-CoV-2 infection. The picture demonstrates how the virus binds to ACE2, triggering IL-6 signaling to activate the JAK/STAT pathway. Phosphorylation of STAT1 and STAT3 results from the activation of JAK1 and TYK2. The potential of MSC-EVs to deliver miRNAs (such as miR-146a, miR-21, and miR-125b) that can alter signaling pathways and lower inflammation is illustrated. The dashed lines indicate possible treatment actions, and the arrows show paths of activation

via the adversely regulating Toll-Like Receptor 4 (TLR4) expression [79].

Conclusion

In summary, this study highlights the therapeutic potential of MSC-derived extracellular vesicles (MSC-EVs) in mitigating COVID-19 pathogenesis by targeting the JAK/STAT signaling pathway. The findings demonstrate that MSC-EVs can inhibit STAT3 activation, thereby reducing the associated cytokine storm and coagulopathy (Fig. 7). These results suggest that MSC-EVs may serve as a promising treatment strategy to improve patient outcomes in COVID-19, warranting further investigation into their mechanisms and clinical applications.

Supplementary Information

The online version contains supplementary material available at https://doi.org/10.1186/s13287-025-04284-8.

Supplementary Material 1.

Acknowledgements
The authors thank you for acknowledging technical and financial support from the Ministry of Education and the University of Hafr Al Batin, Saudi Arabia. Also, we acknowledge the assistance of AI in language editing and paraphrasing. The authors reviewed and approved all final content edited by AI to ensure it reflects our original work.

Author contributions
NE, OB, AAS and HAA designed and planned the study. NE, OB, AAD, ANA and AAS performed the experiments. NE, OB, HAA, AAR, NME and FQA collected the data, and NE, OB, HAA, AAS, NME and RFS analyzed the data. NE, OB and NME wrote the manuscript. All authors read and approved the final manuscript.

Funding
This research was funded by an institutional fund project (Fp-A-2022–2-5–17). Therefore, the authors gratefully acknowledge technical and financial support from the ministry of education and the University of Hafr Al Batin, Saudi Arabia.

Availability of data and materials
The data supporting this study's findings are available from the authors upon reasonable request from the corresponding author.

Declarations

Ethics approval and consent to participate
The National Institutes of Health Guide for the Care and Use of Laboratory Animals (NIH publication No. 85–23, revised 1996) was strictly followed in this investigation. Institutional animal care authorized all protocols and used the Benha University Faculty of Veterinary committee and research ethics board. Project name: IACUCREB, permission number: BUFVTM, approval date: 23/3/2022.

Consent for publication
All authors confirm their consent for publication.

Competing interests
The authors declare that none of the work reported in this study could have been influenced by any known competing financial interests or personal relationships.

Author details
[1]Department of Medical Histology and Cell Biology Faculty of Medicine, Benha University, Benha, Egypt. [2]Stem Cell Unit, Faculty of Medicine, Benha University, Benha, Egypt. [3]Faculty of Medicine, Benha National University, Obour, Egypt. [4]Keele University, Keele, UK. [5]Department of Clinical Laboratory Sciences, College of Applied Medical Sciences, University of Hafr Albatin, Hafar Al-Batin, Saudi Arabia. [6]Department of Clinical Laboratory Sciences, College of Applied Medical Sciences, University of Hafr Al Batin, P.O Box 1803, 31991 Hafr Al Batin, Saudi Arabia. [7]Biology Department, College of Sciences, University of Hafr Al Batin, P. O. Box 1803, 31991 Hafar Al Batin, Saudi Arabia. [8]Molecular Diagnostic Laboratory, Johns Hopkins Aramco Healthcare, 31311 Dhahran, Saudi Arabia. [9]College of Medicine, Alfaisal University, 11533 Riyadh, Saudi Arabia. [10]Department of Public Health and Nutrition, The University of Haripur, Haripur 22610, Pakistan. [11]Department of Medical Histology and Cell Biology, Faculty of Medicine, Zagazig University, Zagazig, Egypt. [12]Department of Medical Biochemistry and Molecular Biology, Faculty of Medicine, Benha University, Banha, Egypt. [13]Anesthesiology & Radiology, Faculty of Vet. Men, Cairo University, P. O. Box 12211, Giza, Egypt. [14]Hormones Department, National Research Centre, Medical Research and Clinical Studies Institute, Cairo, Egypt. [15]Department of Pharmaceutical Chemistry, Faculty of Pharmacy, University of Tabuk, Tabuk, Saudi Arabia. [16]Department of Basic Medical Sciences, College of Medicine, AlMaarefa University, Diriyah, Saudi Arabia. [17]Department of Biochemistry, Faculty of Medicine, Northern Border University, Arar, Saudi Arabia. [18]School of Life Sciences, Keele University Staffordshire, Keele ST5 5BG, UK. [19]Department of Genetics and Genetic Engineering, Faculty of Agriculture, Benha University, Benha, Egypt.

Received: 13 November 2024 Accepted: 19 March 2025
Published online: 15 May 2025

References

1. OMS WHO. Coronavirus (COVID-19) Dashboard. https//covid19 who int/. 2021;
2. Hoffmann M, Kleine-Weber H, Schroeder S, Krüger N, Herrler T, Erichsen S, et al. SARS-CoV-2 cell entry depends on ACE2 and TMPRSS2 and is blocked by a clinically proven protease inhibitor. Cell Elsevier. 2020;181:271–80.
3. Abassi Z, Higazi AAR, Kinaneh S, Armaly Z, Skorecki K, Heyman SN. ACE2, COVID-19 infection, inflammation, and coagulopathy: missing pieces in the puzzle Front Physiol. Front Media. 2020;11:574753.
4. Datta PK, Liu F, Fischer T, Rappaport J, Qin X. SARS-CoV-2 pandemic and research gaps: Understanding SARS-CoV-2 interaction with the ACE2 receptor and implications for therapy. Theranostics. 2020;10:7448.
5. Clarke NE, Turner AJ. Angiotensin-converting enzyme 2: the first decade. Int J Hypertens. Hindawi; 2012;2012.
6. Ravid JD, Leiva O, Chitalia VC. Janus kinase signaling pathway and its role in COVID-19 inflammatory, vascular, and thrombotic manifestations. Cells. 2022;11:306.
7. Matsuyama T, Kubli SP, Yoshinaga SK, Pfeffer K, Mak TW. An aberrant STAT pathway is central to COVID-19. Cell Death Differ. 2020;27:3209–25.
8. Jayaramayya K, Mahalaxmi I, Subramaniam MD, Raj N, Dayem AA, Lim KM, et al. Immunomodulatory effect of mesenchymal stem cells and mesenchymal stem-cell-derived exosomes for COVID-19 treatmen. BMB Rep. 2020;53:400.
9. Lindsay MA. microRNAs and the immune response. Trends Immunol Elsevier. 2008;29:343–51.
10. Nahand JS, Vandchali NR, Darabi H, Doroudian M, Banafshe HR, Moghoofei M, et al. Exosomal microRNAs: novel players in cervical cancer. Epigenomics Future Medicine. 2020;12:1651–60.
11. Khalaj K, Figueira RL, Antounians L, Lauriti G, Zani A. Systematic review of extracellular vesicle-based treatments for lung injury: are EVs a potential therapy for COVID-19? J Extracell Vesicles. 2020;9:1795365.
12. Das K, Rao LVM. The role of microRNAs in inflammation. Int J Mol Sci. 2022;23:15479.
13. Chandan K, Gupta M, Sarwat M. Role of host and pathogen-derived microRNAs in immune regulation during infectious and inflammatory diseases. Front Immunol. 2020;10:3081.
14. Arghiani N, Nissan T, Matin MM. Role of microRNAs in COVID-19 with implications for therapeutics. Biomed Pharmacother. 2021;144:112247.
15. Al Saihati HA, Dessouky AA, Salim RF, Elgohary I, El-Sherbiny M, Ali FEM, et al. MSC–extracellular vesicle microRNAs target host cell-entry receptors in COVID-19: in silico modeling for in vivo validation. Stem Cell Res Ther Springer. 2024;15:316.
16. Bahr MM, Amer MS, Abo-EL-Sooud K, Kamel SM, Fouly MA, Abdallah AN. Effect of topical application of Lyophilized Xenogenous Mesenchymal Stem Cell-Derived Extracellular vesicles on Central and Peripheral corneal ulcers healing in rabbits. Adv Anim Vet Sci. 2023;11:132–40.
17. Rafat A, Gadallah SM, Misk TN, Fadel MS, Abdallah AN, Sharshar A. Potential regenerative effect of mesenchymal stem cells-derived microvesicles on healing of the ruptured achilles tendon in a dog model. J Curr Vet Res. 2022;4:140–51.
18. Imai M, Iwatsuki-Horimoto K, Hatta M, Loeber S, Halfmann PJ, Nakajima N, et al. Syrian hamsters as a small animal model for SARS-CoV-2 infection and countermeasure development. Proc Natl Acad Sci. 2020;117:16587–95.
19. Ebrahim N, Ahmed IA, Hussien NI, Dessouky AA, Farid AS, Elshazly AM, et al. Mesenchymal stem cell-derived exosomes ameliorated diabetic nephropathy by autophagy induction through the mTOR signaling pathway. Cells. 2018;7:226.
20. Teilmann AC, Nygaard Madsen A, Holst B, Hau J, Rozell B, Abelson KSP. Physiological and pathological impact of blood sampling by retro-bulbar sinus puncture and facial vein phlebotomy in laboratory mice. PLoS One. 2014;9:e113225.
21. Ebrahim N, Abd El-Halim HE, Helal OK, El-Azab NE-E, Badr OAM, Hassouna A, et al. Effect of bone marrow mesenchymal stem cells-derived exosomes on diabetes-induced retinal injury: Implication of Wnt/b-catenin signaling pathway. Biomed Pharmacother. 2022;154:113554.
22. Kim S. Bancroft's Theory and Practice of histological techniques eighth edition/S. Kim Suvarna. Elsevier Limited; 2019.
23. Suvarna KS, Layton C, Bancroft JD. Bancroft's theory and practice of histological techniques E-Book. Elsevier health sciences; 2018.
24. Schindelin J, Arganda-Carreras I, Frise E, Kaynig V, Longair M, Pietzsch T, et al. Fiji: an open-source platform for biological-image analysis. Nat Methods. 2012;9:676–82.
25. Bankhead P, Loughrey MB, Fernández JA, Dombrowski Y, McArt DG, Dunne PD, et al. QuPath: open source software for digital pathology image analysis. Sci Rep Nature Publishing Group. 2017;7:1–7.
26. Montazersaheb S, Hosseiniyan Khatibi SM, Hejazi MS, Tarhriz V, Farjami A, Ghasemian Sorbeni F, et al. COVID-19 infection: an overview on cytokine storm and related interventions. Virol J BioMed Central. 2022;19:1–15.
27. Satarker S, Tom AA, Shaji RA, Alosious A, Luvis M, Nampoothiri M. JAK-STAT pathway inhibition and their implications in COVID-19 therapy. Postgrad Med Taylor & Francis. 2021;133:489–507.
28. Asgarpour K, Shojaei Z, Amiri F, Ai J, Mahjoubin-Tehran M, Ghasemi F, et al. Exosomal microRNAs derived from mesenchymal stem cells: cell-to-cell messages. Cell Commun Signal BioMed Central. 2020;18:1–16.
29. Canas CA, Canas F, Bautista-Vargas M, Bonilla-Abadia F. Role of tissue factor in the pathogenesis of COVID-19 and the possible ways to inhibit it. Clin Appl Thromb. 2021;27:10760296211003984.
30. Cesari M, Pahor M, Incalzi RA. Plasminogen activator inhibitor-1 (PAI-1): a key factor linking fibrinolysis and age-related subclinical and clinical conditions. Cardiovasc Ther Wiley Online Library. 2010;28:e72-91.
31. Gupta A, Kashte S, Gupta M, Rodriguez HC, Gautam SS, Kadam S. Mesenchymal stem cells and exosome therapy for COVID-19: current status and future perspective. Hum Cell Springer. 2020;33:907–18.
32. Wathelet MG, Orr M, Frieman MB, Baric RS. Severe acute respiratory syndrome coronavirus evades antiviral signaling: role of nsp1 and rational design of an attenuated strain. J Virol Am Soc Microbiol. 2007;81:11620–33.
33. Bharadwaj U, Kasembeli MM, Robinson P, Tweardy DJ. Targeting janus kinases and signal transducer and activator of transcription 3 to treat inflammation, fibrosis, and cancer: rationale, progress, and caution. Pharmacol Rev ASPET. 2020;72:486–526.

34. Wang J, Schreiber RD, Campbell IL. STAT1 deficiency unexpectedly and markedly exacerbates the pathophysiological actions of IFN-α in the central nervous system. Proc Natl Acad Sci. 2002;99:16209–14.
35. Shao W-H, Gamero AM, Zhen Y, Lobue MJ, Priest SO, Albandar HJ, et al. Stat1 regulates lupus-like chronic graft-versus-host disease severity via interactions with Stat3. J Immunol American Association of Immunologists. 2015;195:4136–43.
36. Avalle L, Pensa S, Regis G, Novelli F, Poli V. STAT1 and STAT3 in tumorigenesis: a matter of balance. Jak-stat Taylor & Francis. 2012;1:65–72.
37. Salman AA, Waheed MH, Ali-**A**bdulsahib AA, Atwan ZW. Low type I interferon response in COVID-19 patients: interferon response may be a potential treatment for COVID-19. Biomed Rep. 2021;14:1–5.
38. Song P, Li W, Xie J, Hou Y, You C. Cytokine storm induced by SARS-CoV-2. Clin Chim acta. 2020;509:280–7.
39. Thorne LG, Bouhaddou M, Reuschl A-K, Zuliani-Alvarez L, Polacco B, Pelin A, et al. Evolution of enhanced innate immune evasion by SARS-CoV-2. Nature. 2022;602:487–95.
40. Ferrario CM, Jessup J, Chappell MC, Averill DB, Brosnihan KB, Tallant EA, et al. Effect of angiotensin-converting enzyme inhibition and angiotensin II receptor blockers on cardiac angiotensin-converting enzyme 2. Circulation Am Heart Assoc. 2005;111:2605–10.
41. Magalhaes GS, Rodrigues-Machado M da G, Motta-Santos D, Campagnole-Santos MJ, Santos RAS. Activation of Ang-(1–7)/Mas receptor is a possible strategy to treat coronavirus (SARS-CoV-2) infection. Front Physiol. Frontiers Media SA; 2020;11:730.
42. Khatri M, Richardson LA, Meulia T. Mesenchymal stem cell-derived extracellular vesicles attenuate influenza virus-induced acute lung injury in a pig model. Stem Cell Res Ther Springer. 2018;9:1–13.
43. Cermak J, Key NS, Bach RR, Balla J, Jacob HS, Vercellotti GM. C-reactive protein induces human peripheral blood monocytes to synthesize tissue factor. 1993;
44. Douglas IS, del Valle FD, Winn RA, Voelkel NF. β-Catenin in the fibroproliferative response to acute lung injury. Am J Respir Cell Mol Biol. 2006;34:274–85.
45. Yamamoto K, Takeshita K, Kojima T, Takamatsu J, Saito H. Aging and plasminogen activator inhibitor-1 (PAI-1) regulation: implication in the pathogenesis of thrombotic disorders in the elderly. Cardiovasc Res Elsevier Science. 2005;66:276–85.
46. Katz JM, Tadi P. Physiology, Plasminogen Activation. 2019;
47. Wu YP, Wei R, Liu ZH, Chen B, Lisman T, Ren DL, et al. Analysis of thrombotic factors in severe acute respiratory syndrome (SARS) patients. Thromb Haemost Schattauer GmbH. 2006;96:100–1.
48. Zhao X, Nicholls JM, Chen Y-G. Severe acute respiratory syndrome-associated coronavirus nucleocapsid protein interacts with Smad3 and modulates transforming growth factor-β signaling. J Biol Chem ASBMB. 2008;283:3272–80.
49. Kaur P, Reis MD, Couchman GR, Forjuoh SN, Greene JF Jr, Asea A. SERPINE 1 links obesity and diabetes: a pilot study. J Proteomics Bioinform. 2010;3:191.
50. Jacobs A, Schutte AE, Ricci C, Pieters M. Plasminogen activator inhibitor-1 activity and the 4G/5G polymorphism are prospectively associated with blood pressure and hypertension status. J Hypertens LWW. 2019;37:2361–70.
51. Healy AM, Pickard MD, Pradhan AD, Wang Y, Chen Z, Croce K, et al. Platelet expression profiling and clinical validation of myeloid-related protein-14 as a novel determinant of cardiovascular events. Circulation Am Heart Assoc. 2006;113:2278–84.
52. Yang Y, Ye W-L, Zhang R-N, He X-S, Wang J-R, Liu Y-X, et al. The role of TGF-β signaling pathways in cancer and its potential as a therapeutic target. Evidence-Based Complement Altern Med. 2021;2021:6675208.
53. Verdecchia P, Cavallini C, Spanevello A, Angeli F. The pivotal link between ACE2 deficiency and SARS-CoV-2 infection. Eur J Intern Med Elsevier. 2020;76:14–20.
54. Li W, Xie L, He X, Li J, Tu K, Wei L, et al. Diagnostic and prognostic implications of microRNAs in human hepatocellular carcinoma. Int J cancer. 2008;123:1616–22.
55. Yeh H-H, Chang W-T, Lu K-C, Lai W-W, Liu H-S, Su W-C. Upregulation of tissue factor by activated Stat3 contributes to malignant pleural effusion generation via enhancing tumor metastasis and vascular permeability in lung adenocarcinoma. PLoS One. Public Library of Science San Francisco, USA; 2013;8:e75287.
56. Beck-Schimmer B, Schwendener R, Pasch T, Reyes L, Booy C, Schimmer RC. Alveolar macrophages regulate neutrophil recruitment in endotoxin-induced lung injury. Respir Res Springer. 2005;6:1–14.
57. McQuattie-Pimentel AC, Budinger GRS, Ballinger MN. Monocyte-derived alveolar macrophages: the dark side of lung repair? Am J Respir Cell Mol Biol. 2018;58:5–6.
58. Johnston LK, Rims CR, Gill SE, McGuire JK, Manicone AM. Pulmonary macrophage subpopulations in the induction and resolution of acute lung injury. Am J Respir Cell Mol Biol. 2012;47:417–26.
59. Gupta KK, Xu Z, Castellino FJ, Ploplis VA. Plasminogen activator inhibitor-1 stimulates macrophage activation through Toll-like Receptor-4. Biochem Biophys Res Commun. 2016;477:503–8.
60. Kutz SM, Hordines J, McKeown-Longo PJ, Higgins PJ. TGF-β1-induced PAI-1 gene expression requires MEK activity and cell-to-substrate adhesion. J Cell Sci. 2001;114:3905–14.
61. Zhu C, Shen H, Zhu L, Zhao F, Shu Y. Plasminogen activator inhibitor 1 promotes immunosuppression in human non-small cell lung cancers by enhancing TGF-**B**1 expression in macrophage. Cell Physiol Biochem. 2018;44:2201–11.
62. Wen M, Men R, Liu X, Yang L. Involvement of miR-30c in hepatic stellate cell activation through the repression of plasminogen activator inhibitor-1. Life Sci. 2016;155:21–8.
63. Valade G, Libert N, Martinaud C, Vicaut E, Banzet S, Peltzer J. Therapeutic potential of mesenchymal stromal cell-derived extracellular vesicles in the prevention of organ injuries induced by traumatic hemorrhagic shock. Front Immunol. 2021;12:749659.
64. Liu P, Yang S, Shao X, Li C, Wang Z, Dai H, et al. Mesenchymal stem cells-derived exosomes alleviate acute lung injury by inhibiting alveolar macrophage pyroptosis. Stem Cells Transl Med. 2024;13:371–86.
65. Ashrafizadeh M, Kumar AP, Aref AR, Zarrabi A, Mostafavi E. Exosomes as promising nanostructures in diabetes mellitus: from insulin sensitivity to ameliorating diabetic complications. Int J Nanomedicine. 2022;1229–53.
66. Gatti S, Bruno S, Deregibus MC, Sordi A, Cantaluppi V, Tetta C, et al. Microvesicles derived from human adult mesenchymal stem cells protect against ischaemia–reperfusion-induced acute and chronic kidney injury. Nephrol Dial Transplant Oxford University Press. 2011;26:1474–83.
67. Chen W. A potential treatment of COVID-19 with TGF-β blockade. Int J Biol Sci. Ivyspring International Publisher; 2020;16:1954.
68. Walton KL, Johnson KE, Harrison CA. Targeting TGF-β mediated SMAD signaling for the prevention of fibrosis. Front Pharmacol. Frontiers Media SA; 2017;8:461.
69. Taganov KD, Boldin MP, Chang K-J, Baltimore D. NF-κB-dependent induction of microRNA miR-146, an inhibitor targeted to signaling proteins of innate immune responses. Proc Natl Acad Sci. National Acad Sciences; 2006;103:12481–6.
70. Yan L-X, Huang X-F, Shao Q, Huang M-Y, Deng L, Wu Q-L, et al. MicroRNA miR-21 overexpression in human breast cancer is associated with advanced clinical stage, lymph node metastasis and patient poor prognosis. Rna Cold Spring Harbor Lab. 2008;14:2348–60.
71. O'Connell RM, Taganov KD, Boldin MP, Cheng G, Baltimore D. MicroRNA-155 is induced during the macrophage inflammatory response. Proc Natl Acad Sci. 2007;104:1604–9.
72. Sheedy FJ, Palsson-McDermott E, Hennessy EJ, Martin C, O'leary JJ, Ruan Q, et al. Negative regulation of TLR4 via targeting of the proinflammatory tumor suppressor PDCD4 by the microRNA miR-21. Nat Immunol. 2010;11:141–7.
73. Bhaumik D, Scott GK, Schokrpur S, Patil CK, Orjalo AV, Rodier F, et al. MicroRNAs miR-146a/b negatively modulate the senescence-associated inflammatory mediators IL-6 and IL-8. Aging. 2009;1:402.
74. Perry MM, Moschos SA, Williams AE, Shepherd NJ, Larner-Svensson HM, Lindsay MA. Rapid changes in microRNA-146a expression negatively regulate the IL-1β-induced inflammatory response in human lung alveolar epithelial cells. J Immunol. 2008;180:5689–98.
75. Zhu N, Zhang D, Chen S, Liu X, Lin L, Huang X, et al. Endothelial enriched microRNAs regulate angiotensin II-induced endothelial inflammation and migration. Atherosclerosis. 2011;215:286–93.
76. Webster RJ, Giles KM, Price KJ, Zhang PM, Mattick JS, Leedman PJ. Regulation of epidermal growth factor receptor signaling in human cancer cells by microRNA-7. J Biol Chem ASBMB. 2009;284:5731–41.

77. Cao M, Seike M, Soeno C, Mizutani H, Kitamura K, Minegishi Y, et al. MiR-23a regulates TGF-β-induced epithelial-mesenchymal transition by targeting E-cadherin in lung cancer cells. Int J Oncol. 2012;41:869–75.
78. Wu W, Takanashi M, Borjigin N, Ohno SI, Fujita K, Hoshino S, et al. MicroRNA-18a modulates STAT3 activity through negative regulation of PIAS3 during gastric adenocarcinogenesis. Br J Cancer. 2013;108:653–61.
79. Tan Y, Yu L, Zhang C, Chen K, Lu J, Tan L. miRNA-146a attenuates inflammation in an in vitro spinal cord injury model via inhibition of TLR4 signaling. Exp Ther. 2018;16:3703–9.

Publisher's Note